Identification of a functional site on the type I TGF-β receptor by mutational analysis of its ectodomain

Alain Guimond[1], Traian Sulea[1], John C. Zwaagstra, Irena Ekiel, Maureen D. O'Connor-McCourt*

Biotechnology Research Institute, National Research Council of Canada, 6100 Royalmount Avenue, Montréal, QC, Canada H4P 2R2

Received 7 November 2001; accepted 12 November 2001

First published online 21 January 2002

Edited by Veli-Pekka Lehto

Abstract Six charged amino acid residues located in the ectodomain of the full-length type I transforming growth factor (TGF)-β receptor were individually mutated to alanine. Mutation of residues D47, D98, K102 and E104 resulted in functionally impaired receptors as demonstrated by a marked decrease in ligand-dependent signaling and ligand internalization relative to the wild-type receptor. The other two mutants (K39A and K87A) exhibited wild-type-like activity. Molecular modeling indicates that the four functionally important residues are located on the convex face of the ectodomain structure. Since mutation of these four residues affects signaling and ligand internalization but not ligand binding, we propose that this functional site is an interacting site between type I and II receptors.

Key words: Type I transforming growth factor-β receptor ectodomain; Mutagenesis; Signaling; Internalization; Homology modeling; Structure–function analysis

1. Introduction

The transforming growth factor-β (TGF-β) superfamily of proteins are key regulators of a wide variety of cellular processes including cell proliferation, differentiation, extracellular matrix deposition and development [1–4]. The signaling events initiated by these growth factors are mediated through two transmembrane receptors that possess serine/threonine kinase activity [5]. It has been established that TGF-β, a 25 kDa dimer, binds to the type II TGF-β receptor (TβRII) which then phosphorylates the type I TGF-β receptor (TβRI) [6,7]. This phosphorylation event activates TβRI, the major signaling receptor, which can then trigger several signaling pathways by activating downstream targets such as the Smad family of proteins [8–10].

Two models have been proposed for the mechanism of formation and activation of the heteromeric TGF-β/TβRII/TβRI ligand–receptor complex. The first model involves binding of the TGF-β ligand to the type II TGF-β receptor ectodomain (TβRII-ECD) which then recruits the type I TGF-β receptor ectodomain (TβRI-ECD) to form an active ligand–receptor complex [6,7]. A second more recent model proposes that TβRI and TβRII form an inactive receptor complex in the absence of ligand and that TGF-β binding induces a relative reorientation of TβRI-ECD and TβRII-ECD that allows productive alignment of the intracellular kinase domains of the two receptors [11,12]. Thus, it is clear that the ectodomains of TβRI and TβRII play an important role in modulating TGF-β signaling. However, the specific amino acid residues involved in the underlying intermolecular interactions within the TGF-β/TβRII-ECD/TβRI-ECD complex are presently unknown due to the lack of relevant structural and functional data.

In this study, TβRI was subjected to alanine point mutagenesis in order to identify functional amino acid residues on its ectodomain. Six charged residues located in the TβRI-ECD were individually mutated to alanine. Targeting of charged residues was motivated, firstly, by a reduced susceptibility to global alteration of the domain structure upon mutation since charged side chains are often exposed to the solvent at the protein surface. Secondly, it is widely accepted that electrostatic interactions are important for molecular binding and recognition. Analysis of atomic resolution structures has shown that protein–protein interfaces are rich in polar and charged side chains that generally participate in hydrogen bond interactions [13]. Currently, there is a growing consensus that electrostatic interactions are likely to enhance binding specificity although they do not necessarily contribute strongly to binding affinity [14–20].

We first characterized the TβRI mutants for their level of expression at the cell surface as well as for the efficiency of their affinity cross-linking to the TGF-β1 ligand in the presence of TβRII. The functional competency of mutant TβRIs was assessed independently in ligand-induced signaling and ligand endocytosis experiments. One of the six point mutations to alanine altered significantly the TβRI/ligand cross-linking efficiency. Four of the six mutants displayed marked reductions in ligand-dependent signaling as well as in the level of ligand internalization. The three-dimensional structure of the TβRI-ECD was modeled based on the recently determined crystal structure of the homologous type IA bone morphogenetic protein receptor ectodomain (BRIA-ECD) in complex with the bone morphogenetic protein 2 (BMP-2) ligand [21]. The TβRI-ECD model is used as a framework for structural

*Corresponding author. Fax: (1)-514-496-5143.
E-mail address: maureen.o'connor@nrc.ca (M.D. O'Connor-McCourt).

[1] These authors contributed equally to this work.

Abbreviations: TβRI-ECD, type I TGF-β receptor ectodomain; TβRII-ECD, type II TGF-β receptor ectodomain; TGF-β, transforming growth factor-β

0014-5793/02/$22.00
PII: S0014-5793(01)03231-8

and mechanistic interpretation of the data resulting from this first functional mutagenesis investigation of the ectodomain of TβRI.

2. Materials and methods

2.1. Plasmids and mutagenesis

The full-length rat TGF-β receptor type I cDNA (GenBank accession number L26110) was subcloned at the *Eco*RI site of pcDNA-3 (Invitrogen) to yield p3TβR1. A 1.1-kbp *Kpn*I fragment was further subcloned in pBluescript SK (Stratagene) to produce pBTβR1K. An N-terminal 6×His tag was added by ligating a double stranded oligonucleotide (5′-TGGACATCACCACCATCATCACGC) at the *Sma*I site (position 113) just after the signal peptide. This plasmid was then used as a template for site directed mutagenesis according to Barettino et al. [22]. The anchor-T7 primer is 5′-GACTCGAGTCGACATCGTAATACGACTCACTATAGGG; the anchor specific primer corresponds to the first 17 bases of the former primer. Mutagenic primers complementary to the coding strand were as follows (mutated bases are underlined): K39A = 5′-AAAATTGTCCGCTGTACAGAGG, K47A = 5′-GCAGAGACCAGCTGTCTCAC, K87A = 5′-GCCCCTGTTGCTGAAGATGG, D98A = 5′-TGCAGTGAGCCTGATTGC, K102A = 5′-GGGAGTTCTATTGCATTGCAGTG, E104A = 5′-AGTTGGGAGTGCTATTTTAT.

Amplification products were purified (Qiaquick-PCR, Qiagen), and cloned in the pBTβR1K plasmid as a 325 bp *Nco*I–*Ppu*MI fragment using standard procedures. Clones that contained mutations were selected by dideoxy sequencing (Pharmacia), and subcloned back into the original expression plasmid (p3TβR1) as *Kpn*I fragments.

2.2. Cell culture and transfections

HEK 293 cells, and Mink Lung Epithelial R1-B/L-17 cells were maintained in Dulbecco's modified Eagle's medium (DMEM) supplemented with 10% fetal bovine serum (FBS). 293 cells were seeded in 12 well plates (1×10^5 cells/well) or 60 mm dishes (4×10^5 cells/well) and transfected with SuperFect transfection reagent (Qiagen) according to the manufacturer's protocol. R1-B cells were seeded in 60 mm dishes (4×10^5 cells/well) and also transfected with SuperFect reagent. After 3 h of incubation, the transfection reagent was removed and replaced with fresh complete media.

2.3. Surface expression

293 cells were transfected using 2 μg of DNA and 5 μl of SuperFect reagent according to the manufacturer's protocol. 48 h after transfection the cells were suspended in cold DMEM-10% FBS for 30 min on ice and then incubated 1 h on ice in the presence of an anti-6×His monoclonal antibody (Clontech) diluted 1:1000. After a wash in cold DMEM-10% FBS, cells were incubated 1 h on ice with a FITC conjugate Goat anti-mouse Fcγ fragment specific IgG (Jackson) diluted 1:100. Cells were then washed in cold DMEM-10% FBS and analyzed by flow cytometry on an EPIC® XL–MCS (Beckman/Coulter®).

2.4. Affinity cross-linking

[^{125}I]TGF-β1 was purchased from NEN Life Sciences Products. 293 cells were transfected with 1.5 μg of DNA at a 1:1 ratio of wild-type or mutant TβRI DNA to wild-type TβRII DNA using SuperFect reagent (Qiagen). 48 h after transfection the cells were incubated with 150 pM of [^{125}I]TGF-β1 on ice for 3 h and receptor-bound ligand was cross-linked with BS^3 (Pierce) as previously described [23]. Labeled receptors were then solubilized in 1% Triton X-100, 10% glycerol, 20 mM Tris pH 7.4, 1 mM EDTA. Iodinated ligand–receptor complexes were resolved on 4–12% gradient SDS–PAGE, and the gel fixed in methanol–acetic acid, dried and exposed on a phosphorimager screen.

2.5. Signaling assay

R1-B cells were cotransfected with wild-type or mutant TβRI DNA, luciferase reporter DNA (p3TP-Lux) and green fluorescent protein DNA (GFPq, Quantum Biotechnology) to normalize for transfection efficiency. After transfection, the cells were split in two aliquots. The first aliquot was used for the signaling assay. 24 h after transfection, the cells were incubated 3 h in serum-free medium, then treated or not with 150 pM of TGF-β1 (R&D Systems) for 16 h. Cells were then lysed in 100 μl of cell culture lysis reagent and 20 μl aliquots were used to measure luciferase activity (Promega, luciferase assay system) on a Lumat LB9501 (Berthold) for 20 s. A DNA ratio of 2:9:1 for TβRI:p3TP-lux:GFPq was used. The second aliquot was analyzed by flow cytometry on an EPICS® XL-MCS (Beckman/Coulter®) and the total fluorescence value was used to normalize for transfection efficiency.

2.6. Ligand internalization assay

293 cells were transfected with the plasmids expressing wild-type or mutant TβRI and wild-type TβRII using SuperFect reagent (Qiagen) according to the manufacturer's specifications. After 20 h the cells were tested for internalization of [^{125}I]TGF-β1. Cells were washed twice with TGF-β binding media (200 mM HEPES-buffered DMEM pH 7.4, 0.2% bovine serum albumin (BSA)) and then incubated in binding media for 30 min at 4°C. Cells were then treated with 100 pM [^{125}I]TGF-β1 in cold binding media plus or minus unlabeled 10 nM TGF-β1 and immediately transferred to a 37°C water bath for 90 min. Control time course assays indicated that the amount of TGF-β1 internalized was maximal within this time period (data not shown). Cells were then transferred on ice and washed twice with Dulbecco's phosphate-buffered saline containing 0.9 mM $CaCl_2$, 0.5 mM $MgCl_2$ (D-PBS^{2+}) and 0.1% BSA. Surface ligand was removed from the cells by washing twice with 150 mM NaCl, 0.1% acetic acid at 4°C for 2 min each. Internalized ligand was then extracted in solubilization buffer (1.0% Triton-X-100, 10% glycerol, 1 mM EDTA, 20 mM Tris–HCl pH 7.5) for 30 min at 4°C. The amount of internalized ligand was quantified in a gamma counter. Specific counts (specific cpm) were determined by subtracting competed samples (plus unlabeled TGF-β1) from non-competed samples.

2.7. Statistics

Data were analyzed by one-way analysis of variance using $P > 0.05$ as significance criterion. Post-hoc analysis relied on Dunnet's Multiple Comparison Test using the Prism software (GraphPad Software Inc.).

2.8. Molecular modeling

The three-dimensional structure of human TβRI-ECD (residues G30–P119) was predicted by combining homology modeling with conformational sampling. Homology modeling was carried out using the program COMPOSER [24] implemented in SYBYL 6.6 molecular modeling software (Tripos). The 2.9 Å resolution crystal structure of type IA bone morphogenetic protein receptor ectodomain (BRIA-ECD) determined in complex with the BMP-2 ligand [21] (PDB entry 1ES7) was used as a template. The conserved pattern of 10 cysteine residues in the target/template sequence alignment (Fig. 1) allowed formation of five disulfide bonds in TβRI-ECD based on the disulfide connectivity observed in BRIA-ECD structure. Five structurally conserved regions (SCRs) and four intervening structurally variable regions (SVRs, i.e. loops with different length in TβRI-ECD and BRIA-ECD) were assigned in order to build a preliminary model of TβRI-ECD (Fig. 1). An initial conformation for each SVR was constructed by searching a database of protein structures deposited in PDB. Structural refinement was done by energy minimization in SYBYL 6.6 using the AMBER 4.1 all-atom force field [25] with the Powel minimizer, a distance-dependent (4*R*) dielectric constant, an 8 Å nonbonded cutoff, and a root mean square difference (RMSD) gradient of 0.05 kcal/mol Å (these settings were also used in the conformational search refinement stage, see below). Sequential energy minimization runs were carried out in order to allow a gradual relaxation of the structure, starting with SVRs, then including the side chains of SCRs, and finally energy minimizing the entire structure.

The SVRs in the resulting TβRI-ECD model were refined by conformational search using the Monte Carlo minimization (MCM) approach [26–29]. The sampling region (SR) was composed of the loops H39–F46 (SR-I), T61–K64 (SR-II) and E74–R82 (SR-III), thus covering all SVRs (Fig. 1). In each MCM cycle, a starting conformation of the protein was generated by randomly perturbing one or more dihedral angles in the SR. These perturbations involved random changes in the side chain dihedral angles and crankshaft rotations around the peptide units. Disulfide bonds as well as the C-terminal peptide bond at each of the three sampled loops were broken prior to backbone dihedral angle rotations and re-formed for energy minimization. The starting conformation then was subjected to an AMBER 4.1 energy minimization in which only the backbone atoms of the residues forming the β-sheets of the domain, (which belong to the SCRs) were kept

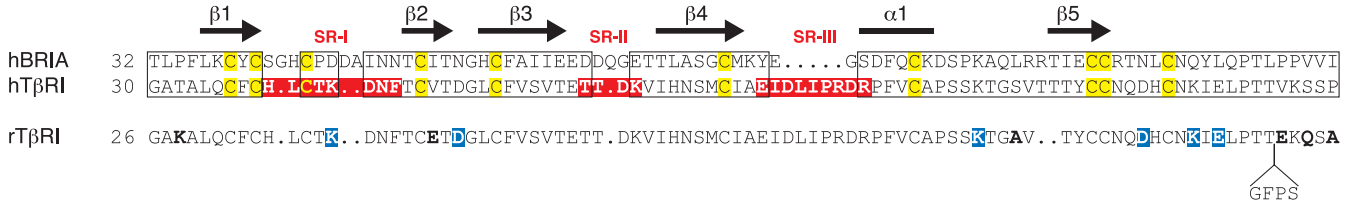

Fig. 1. Sequence alignment used in the modeling of the human TβRI-ECD structure. Secondary structural elements observed in the crystal structure of the BRIA-ECD template are shown and labeled. Cysteine residues are highlighted in yellow. Structurally conserved regions (SCRs) assigned in the initial model building are enclosed in boxes. Non-homologous loops of TβRI-ECD included in the MCM sampling region (SR) are highlighted on red background and labeled SR-I to III. The sequence of rat TβRI-ECD, used in our experiments, is also aligned, with the residues that were mutated to alanine highlighted on blue background, and with the residues that are different in the human TβRI-ECD sequence indicated in bold. The position of a four amino acid insertion in the rat sequence is also shown.

rigid. The decision of accepting or rejecting the resulting conformation was taken on energy basis according to the Metropolis probability criterion. An accepted conformation or a rejected conformation whose internal energy was within 10 kcal/mol above the internal energy of the current accepted conformation was stored in a database after passing through the chirality and RMSD-based conformer redundancy filters. A total of 30 000 MCM cycles were carried out to generate a database of energy-ranked feasible conformations of the domain structure. The quality of the TβRI-ECD model corresponding to the lowest energy conformation was assessed with the PROCHECK program [30] and the PROTABLE module in SYBYL 6.6.

3. Results and discussion

3.1. Expression of mutant TβRIs and formation of mutant TβRI/TβRII complexes

The surface expression of wild-type and mutant TβRIs was monitored by flow cytometry in transiently transfected 293 cells using an antibody directed against a 6×His tag added to the N-terminus of each receptor. Expression of mutant TβRIs varied between 82% and 91% relative to wild-type TβRI (Fig. 2). TβRI forms a heteromeric receptor complex with TβRII and can be affinity cross-linked to the ligand only in the presence of TβRII. Therefore, ligand binding properties of the wild-type and mutant TβRIs were investigated in order to assess the formation of mutant TβRI/TβRII complexes.

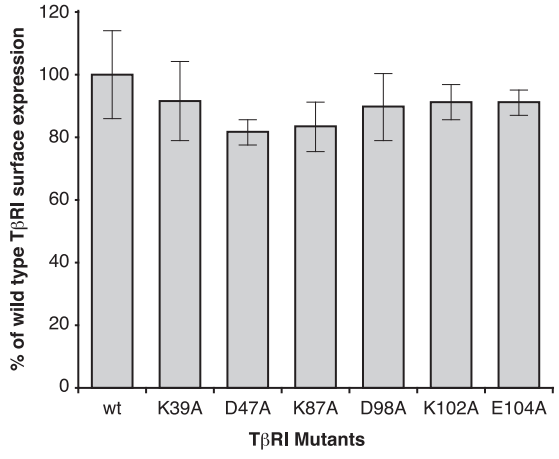

Fig. 2. Surface expression of TβRI mutants. Transiently transfected 293 cells were incubated with an antibody directed against the N-terminal 6×His tag on TβRI and detected by flow cytometry analysis with an FITC-conjugated secondary antibody (see Section 2). Histograms show the mean fluorescence values calculated from four independent experiments.

Each TβRI was cotransfected with wild-type TβRII in 293 cells followed by affinity cross-linking to 150 pM of [^{125}I]TGF-β1. With one exception, all mutant TβRIs were found to be crossed-linked to ligand in the presence of wild-type TβRII at levels comparable to that of the wild-type TβRI (Fig. 3). One mutant, K87A, was affinity cross-linked with lower efficiency (59% relative to the wild-type). The reduced labeling of this mutant is likely due to the loss of a free amino group that may be required for covalent cross-linking. These results indicate that the mutant TβRIs are efficiently expressed and transported to the cell surface, bind the TGF-β ligand, and form heteromeric receptor complexes in the presence of the ligand.

3.2. Ligand-dependent signaling of mutant TβRI/TβRII complexes

Although receptor heteromerization is necessary for TGF-β signaling, optimal activity also requires formation of a functional heteromeric receptor complex characterized by the cor-

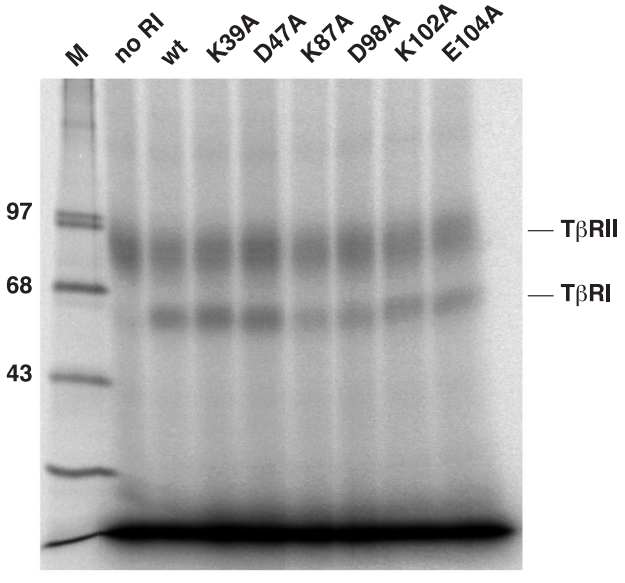

Fig. 3. Affinity cross-linking of TβRI mutants. 293 cells were transiently transfected with TβRII without TβRI or together with wild-type or mutant TβRIs followed by cross-linking to [^{125}I]TGF-β1. Labeled receptors were resolved on 4–12% gradient gels and exposed to phosphorimager screens. Mutants are labeled in the respective lanes. M: molecular weight (kDa).

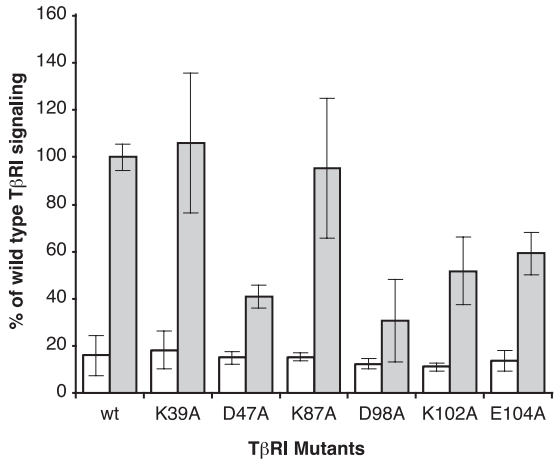

Fig. 4. Signaling by the TβRI mutants. Mink Lung Epithelial R1-B/L-17 cells were transiently cotransfected with a luciferase reporter plasmid and wild-type or mutant TβRIs. Histograms show the level of luciferase activity expressed as percent of wild-type TβRI activity. Data are the mean values obtained from three different experiments. White bars show the signaling of non-treated cells and gray bars the signaling of TGF-β1-treated cells.

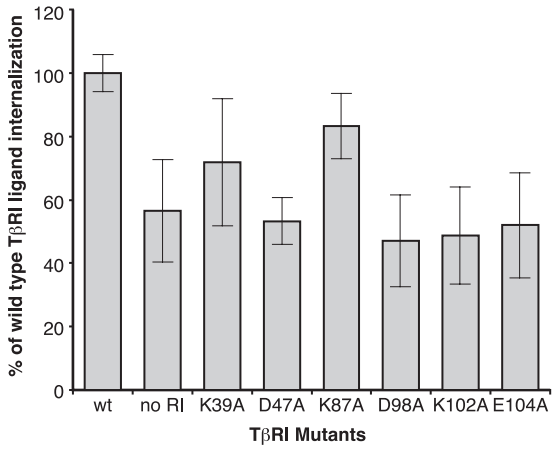

Fig. 5. Internalization of ligand by TβRI mutants. Transiently transfected 293 cells were incubated with [I^{125}]TGF-β1 in the presence (competed) or absence of 100 fold excess of unlabeled TGF-β1. After removing surface-bound ligand, the specific counts from internalized ligand were calculated by subtracting competed samples from total counts (non-competed). Data were obtained from at least three independent experiments and are expressed as percent of wild-type TβRI ligand internalization.

rect alignment of the TβRI and TβRII ectodomains [11,12]. Therefore, wild-type and mutant TβRIs were analyzed for their ability to rescue TGF-β-dependent signaling in Mink Lung Epithelial R1-B/L-17 cells. This cell line lacks cell surface TβRI and therefore TGF-β responsiveness. A reporter plasmid, p3TP-Lux, which contains three copies of the plasminogen activator inhibitor-1 promoter (PAI-1) upstream to the luciferase gene, was cotransfected with wild-type or each mutant TβRI and cell responsiveness was assayed by measuring TGF-β-induced luciferase activity [5]. The results show that none of the mutant TβRIs was entirely defective in signaling. However, their signaling capability varied significantly (Fig. 4). The D98A mutant signaled at the lowest level (30% of wild-type activity), whereas mutants D47A, K102A and E104A retained only 40–60% of the wild-type TβRI activity. In contrast, mutants K39A and K87A were able to rescue signaling at levels comparable to that of the wild-type receptor. These results indicate that, although all mutant TβRIs were able to form heteromeric complexes with TβRII in the presence of the ligand, the stability of the productive TβRI/TβRII complex was reduced upon D98A, D47A, K102A and E104A mutations, but remained unaffected by the K39A and K87A mutations introduced in the TβRI-ECD. The observation that mutant K87A, which was cross-linked with lower

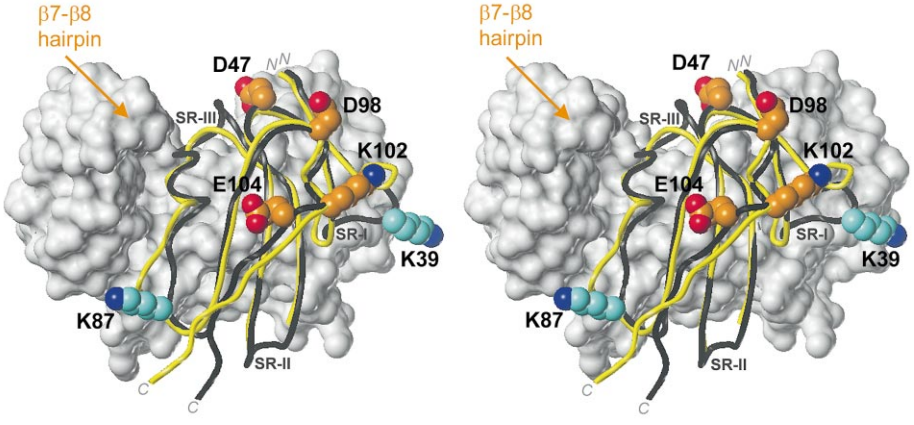

Fig. 6. Stereoview of the structural mapping of the TβRI functional site. The human TβRI-ECD model structure (black tube) and BRIA-ECD crystal structure (yellow tube) are overlaid, with the convex side in front. The structures superimpose with an RMSD of 0.59 Å between the corresponding Cα atoms of the five structurally conserved β-strands. MCM-sampled regions (SRs) of TβRI-ECD are labeled (see also Fig. 1). The side chains (including Cα atoms) of TβRI residues mutated to alanine are shown as CPK models and labeled according to the rat TβRI sequence. The side chains delineating a functional, TβRII-ECD interacting site of TβRI-ECD are shown with orange carbon atoms. The functionally irrelevant side chains are shown with cyan carbon atoms. The Connolly surface of the BMP-2 ligand is displayed relative to the superimposed ectodomains, based on the orientation observed in the crystal structure of the BRIA-ECD/BMP-2 complex. There was no attempt to optimize the interactions in the TβRI-ECD/BMP-2 complex. The tip of the hairpin β7–β8 of the BMP-2 ligand is indicated, in order to highlight the corresponding relative location of a functional, TβRII-ECD interacting site of the TGF-β ligand.

efficiency, rescued signaling at wild-type receptor levels, supports the idea that reduced labeling of this mutant results from less efficient cross-linking rather than a disruption of the heteromeric TβRI/TβRII/ligand complex.

3.3. Ligand internalization by mutant TβRI/TβRII complexes

Using chimeric [31] and wild-type [32] receptors, it has been shown that ligand internalization is optimal when both TβRI and TβRII are coexpressed. Using chimeric receptors it was also shown that the kinase activity of TβRII, but not TβRI, is essential for maximal ligand internalization by the heteromeric receptor complex [31]. These experiments indicate that a ligand internalization assay may be used as an indicator of TβRI/TβRII complex formation, in addition to the affinity cross-linking and signaling assays. Therefore, we employed a [^{125}I]TGF-β1 ligand internalization assay to further analyze the ability of mutant TβRIs to form complexes with TβRII in the presence of TGF-β. As shown in Fig. 5, expression of TβRII alone resulted in a level of ligand internalization that was approximately 55% of the level achieved by coexpressing both wild-type receptors. Similar, low internalization levels were seen in cells coexpressing TβRII along with D47A, D98A, K102A or E104A mutant TβRIs. In contrast, coexpression of either K39A or K87A mutant TβRIs with TβRII resulted in internalization levels comparable to that achieved by coexpression of wild-type TβRI and TβRII. These results parallel those obtained in the signaling assay and indicate that the D47A, D98A, K102A and E104A single point mutations in the TβRI-ECD impair the functionality of the TβRI/TβRII complex with respect to both ligand-dependent signaling and ligand internalization.

3.4. Structure–function relationship analysis of TβRI

Structural mapping of functional sites can provide insights into the mechanisms underlying protein function at the molecular level. The three-dimensional atomic structure of TβRI-ECD has not been determined yet. Recently, the crystal structure of a close homolog of TβRI-ECD, the type IA bone morphogenetic protein receptor ectodomain (BRIA-ECD) has been determined in complex with the BMP-2 ligand [21]. In an earlier study [33], a model of TβRI-ECD has been constructed by homology to protectin (CD59) and refined by a molecular dynamics simulation (PDB entry 1TBI). Here we built a homology model of TβRI-ECD based on the BRIA-ECD structure as a more suitable template in comparison with CD59, and refined the conformation of three non-homologous loop regions using the Monte Carlo sampling with energy minimization (MCM) approach [26–29].

The folding topology stabilized by five disulfide bridges of the TβRI-ECD model is conserved with respect to BRIA-ECD structure [21] (Fig. 6). The region of high structural similarity includes the two β-sheets of the domain (formed by five β-strands) as well as most of the C-terminal stretch of residues. The short α-helix that flanks the central β-sheet is slightly distorted in the TβRI-ECD model as compared with the BRIA-ECD structure, due to proline residues in this region of TβRI-ECD. Lower structural similarity is observed for two of the non-homologous loops included in the MCM SR (SR-I: loop β1-β2 and SR-III: loop β4-α1), for the loop α1-β5, as well as for the C-terminal four amino acid residues. Overall, the modeled TβRI-ECD structure preserves the 'open left hand' topology of the BRIA-ECD structure, with a concave face and a convex face stemming from the curvature of the central β-sheet.

Mapping of the TβRI residues investigated by mutagenesis in this study onto the modeled structure of TβRI-ECD is shown in Fig. 6. All these residues are exposed at the molecular surface, thus suggesting that no major conformational changes would result upon their individual mutation to alanine. This is in agreement with the wild-type levels of cell surface expression observed for the corresponding mutant TβRIs. Residues D47, D98, K102 and E104, which are important for signaling and ligand internalization correspond to structurally conserved regions between the TβRI-ECD model and the BRIA-ECD structure template. These residues are located close to each other on the convex face of the modeled TβRI-ECD structure. In contrast, residues K39 and K87 which are not important for signaling and ligand internalization, are located at the outer edge of the ectodomain structure, between its convex and concave faces. The residue K39 belongs to the loop β1-β2, which was included in the MCM SR (SR-I) and which occupies a more distal position relative to the corresponding, 3-residue longer loop in the BRIA-ECD structure. The residue K87 in the loop α1-β5 was positioned closer to the central β-sheet during model refinement and thus deviates slightly from the location of the equivalent lysine residue in the BRIA-ECD structure.

The overlap between structural and functional clustering indicates the presence of a functional epitope on the convex face of the TβRI-ECD. As demonstrated by our affinity cross-linking experiments, this functional epitope is not involved in ligand binding. Our ligand-dependent signaling and ligand internalization data indicate that this functional epitope of TβRI is implicated in the stability of the productive TβRI/TβRII heteromeric complex and thus, it represents a putative interacting site with the TβRII-ECD. The location of this TβRII-ECD interacting site on the convex face of TβRI-ECD is consistent with a model in which the TβRI-ECD/ligand interaction would be homologous to the observed BRIA-ECD/ligand interaction [21], which occurs on the concave face of the ectodomain. In Fig. 6 we displayed the position of the BMP-2 ligand dimer relative to the superimposed ectodomains of TβRI and BRIA. In this putative binding mode, the functional epitope that we have identified on the TβRI-ECD would not interact with the TGF-β ligand and would be readily available for interaction with TβRII-ECD. As an additional support for this binding mode is the relative positioning of this functional epitope on the TβRI-ECD with respect to the tip of the hairpin β7–β8 of the ligand. In the case of the TGF-β ligand, this hairpin has been shown to form an interacting site with TβRII [34]. Both the ligand site and the TβRI-ECD site could simultaneously contact the ectodomain of TβRII (Fig. 6). It is possible that some other residues of TβRI located on the convex face of the ectodomain and adjacent to those identified here, would contribute to a larger contact interface with TβRII-ECD.

It is worth noting that the K87A mutation resulted in a 40% reduction of TβRI cross-linking to the ligand. In the binding mode proposed in Fig. 6, the K87 side chain would be positioned in close proximity to the ligand, but only partially buried upon complex formation. This suggests that the K87 side chain of TβRI could be readily employed in the covalent cross-linking to the TGF-β1 ligand (e.g. with K26, K31 or K37). Therefore, the decrease in cross-linking effi-

ciency upon K87A mutation could be due to the loss of a free amino group required for the covalent cross-linking. Based on the putative binding mode, it is less probable that the K87A mutation would impair significantly the TβRI-ECD/ligand interaction in the functional heteromeric receptor complex. These hypotheses are fully supported by our ligand-dependent signaling and ligand internalization data, which show a functionally competent K87A mutant TβRI.

Since TGF-β signaling requires ligand stimulation, it is likely that the inter-receptor binding affinity in the productive TβRI-ECD/TβRII-ECD complex, in the absence of the ligand, is weak. This is consistent with our finding of a receptor interacting site formed by charged residues, in which case the intermolecular electrostatic attraction in the complex would be largely offset by the competing desolvation costs incurred upon binding [35,36]. Thus, the residues in the functional epitope of the TβRI-ECD might not contribute strongly to the net binding affinity to TβRII-ECD. Their mutation to alanine, however, would result in sub-optimal electrostatic complementarity in the complex and therefore, in a considerable weakening of the net binding affinity due to under-compensated desolvation penalties [37–39]. Given that TGF-β has a low affinity for TβRI and high affinity for TβRII [6,7], an effective binding of TβRI-ECD to a preformed TβRII-ECD/ligand complex could be achieved upon burial of two large surface, weak affinity interacting sites of TβRI-ECD: one on its concave face for binding to the ligand, and the other one on its the convex face for binding to the TβRII-ECD.

Acknowledgements: The authors would like to acknowledge Lucie Bourget for her help with flow cycometry analysis and André Migneault for preparation of the figures. NRCC publication No. 44797.

References

[1] Roberts, A.B. and Sporn, M.B. (1990) in: Handbook of Experimental Pharmacology. Peptide Growth Factors and Their Receptors (Sporn, M.B. and Roberts, A.B., Eds.), pp. 419–472, Springer-Verlag, New York.
[2] Roberts, A.B. and Sporn, M.B. (1993) Growth Factors 8, 1–9.
[3] ten Dijke, P., Miyazono, K. and Heldin, C.H. (1996) Curr. Opin. Cell Biol. 8, 139–145.
[4] Massagué, J., Attisano, L. and Wrana, J.L. (1994) Trends Cell Biol. 4, 172–178.
[5] Wrana, J.L., Attisano, L., Càrcamo, J., Zentella, A., Doodey, J., Laiho, M., Wang, X.-F. and Massagué, J. (1992) Cell 71, 1003–1014.
[6] Wrana, J.L., Attisano, L., Wieser, R., Ventura, F. and Massagué, J. (1994) Nature 370, 341–347.
[7] ten Dijke, P., Yamashita, H., Ichijo, H., Franzen, P., Laiho, M., Miyazono, K. and Heldin, C.H. (1994) Science 264, 101–104.
[8] Wrana, J.L. and Attisano, L. (1996) Trends Genet. 12, 493–496.
[9] ten Dijke, P., Miyazono, K. and Heldin, C.H. (2000) Trends Biochem. Sci. 25, 64–70.
[10] Massagué, J. and Chen, Y.-G. (2000) Genes Dev. 14, 627–644.
[11] Zhu, H.-J. and Sizeland, A.M. (1999) J. Biol. Chem. 274, 29220–29227.
[12] Zhu, H.-J. and Sizeland, A.M. (1999) J. Biol. Chem. 274, 11773–11781.
[13] Janin, J. and Chothia, C.J. (1990) J. Biol. Chem. 265, 16027–16030.
[14] Hendsch, Z.S. and Tidor, B. (1994) Protein Sci. 3, 211–226.
[15] Yang, A.-S. and Honig, B. (1995) J. Mol. Biol. 252, 351–365.
[16] Wang, L., O'Connell, T., Tropsha, A. and Hermans, J. (1996) Biopolymers 39, 479–489.
[17] Waldburger, C.D., Schildbach, J.F. and Sauer, R.T. (1995) Nat. Struct. Biol. 2, 122–128.
[18] Wimley, W.C., Gawrisch, K., Creamer, T.P. and White, S.H. (1996) Proc. Natl. Acad. Sci. USA 93, 2985–2990.
[19] Sindelar, C.V., Hendsch, Z.S. and Tidor, B. (1998) Protein Sci. 7, 1898–1914.
[20] O'Shea, E.K., Rutkowski, R. and Kim, P.S. (1992) Cell 68, 699–708.
[21] Kirsch, T., Sebald, W. and Dreyer, M.K. (2000) Nat. Struct. Biol. 7, 492–496.
[22] Barettino, D., Feigenbutz, M., Valcarcel, R. and Stunnenberg, H.G. (1994) Nucl. Acids Res. 22, 541–542.
[23] Philip, A. and O'Connor-McCourt, M.D. (1991) J. Biol. Chem. 266, 22290–22296.
[24] Sutcliffe, M.J., Haneef, I., Carney, D. and Blundell, T.L. (1987) Protein Eng. 1, 377–384.
[25] Cornell, W.D., Cieplak, P., Bayly, C.I., Gould, I.R., Merz, K.M., Ferguson, D.M., Spellmeyer, D.C., Fox, T., Caldwell, J.W. and Kollman, P.A. (1995) J. Am. Chem. Soc. 117, 5179–5197.
[26] Li, Z. and Scheraga, H.A. (1987) Proc. Natl. Acad. Sci. USA 84, 6611–6615.
[27] Nägler, D.K., Zhang, R., Tam, W., Sulea, T., Purisima, E.O. and Ménard, R. (1999) Biochemistry 38, 12648–12654.
[28] Therrien, C., Lachance, P., Sulea, T., Purisima, E.O., Qi, H., Ziomek, E., Alvarez-Hernandez, A., Roush, W.R. and Ménard, R. (2001) Biochemistry 40, 2702–2711.
[29] Lin, L.Y.-C., Sulea, T., Szittner, R., Vassilyev, V., Purisima, E.O. and Meighen, E.A. (2001) Protein Sci. 10, 1563–1571.
[30] Laskowski, R.A., MacArthur, M.W., Moss, D.S. and Thornton, J.M. (1993) J. Appl. Cryst. 26, 283–291.
[31] Anders, R.A., Doré Jr., J.J.E., Arline, S.L., Garamszegi, N. and Leof, E.B. (1998) J. Biol. Chem. 273, 23118–23125.
[32] Zwaagstra, J.C., El-Alfy, M. and O'Connor-McCourt, M.D. (2001) J. Biol. Chem. 276, 27237–27245.
[33] Jokiranta, T.S., Tissari, J., Teleman, O. and Meri, S. (1995) FEBS Lett. 376, 31–36.
[34] Burmester, J.K., Qian, S.W., Ohlsen, D., Phan, S., Sporn, M.B. and Roberts, A.B. (1998) Growth Factors 15, 231–242.
[35] Chong, L.T., Dempster, S.E., Hendsch, Z.S., Lee, L.-P. and Tidor, B. (1998) Protein Sci. 7, 206–210.
[36] Sulea, T. and Purisima, E.O. (2001) J. Phys. Chem. B 105, 889–899.
[37] Hendsch, Z.S., Nohaile, M.J., Sauer, R.T. and Tidor, B. (2001) J. Am. Chem. Soc. 123, 1264–1265.
[38] Lee, L.-P. and Tidor, B. (2001) Protein Sci. 10, 362–377.
[39] Lee, L.-P. and Tidor, B. (2001) Nat. Struct. Biol. 8, 73–76.